Highly sensitive D-shaped optical fibre surface plasmon resonance refractive index sensor based on Ag-α-Fe2O3 grating

Riadh A.Kadhim, Liming Yuan, Hao Xu ,Jiang Wu , Senior Member, IEEE, Zhiming Wang

***Abstract*—This work proposed the simulation of a highly sensitive surface plasmon resonance (SPR) optical fibre sensor equipped with a hematite ($\alpha - Fe_2O_3$) layer coated with silver gratings on the surface of a D-shaped optical fibre. $\alpha - Fe_2O_3$ nanomaterial film was utilised as the sensing layer. Free electrons on the metal surface were stimulated via evanescent waves on the fibre surface to generate surface plasmon waves. The resonance absorption peaks were monitored to determine the changes in refractive index (RI). The SPR fibre sensor was optimised using the finite element method to analyse the structural parameters of the D-shaped optical fibre and silver gratings. This method was also applied to examine the effect of the thickness of the hematite sensing layer on sensor sensitivity (S). The hematite-coated silver gratings significantly enhanced the sensor as revealed by the simulation outcomes. In this work, the maximum response S of the sensor can reach 6.4 μm/RIU when the external RI was changed from 1.33 to 1.39 with 45 nm thick silver grating, 50 nm width air gaps and 12 nm thick hematite ($\alpha - Fe_2O_3$). The results suggest the high potential of $\alpha - Fe_2O_3$ nanomaterials in optical fibre-sensing applications.**

***Index Terms*—:optical fibre sensors , silver gratings ,surface plasmon resonance (SPR), hematite ($\alpha - Fe_2O_3$),**

I. Introduction

Biosensors with surface plasmon resonance (SPR) are considered as a leading optical sensing technology because they can be applied in environmental monitoring and medical biochemical and biomolecule diagnostics, among other fields [1], [2], [3]. A metal-dielectric interface that accommodates a p-polarized electromagnetic (EM) wave is present in the optical structure of SPR, and a surface plasmon wave (SPW) runs across this interface. Strong light absorption is caused by energy transfer when the p-polarized light is incident on the metaldielectric interface such that the propagation constant (and energy) owing to the resulting evanescent wave is similar to the SPW. The output signal demonstrates resonance wavelength is a sharp dip at a specific wavelength[4]. A thin metallic layer of either Ag or Au that is directly integrated onto a coupling prisms base[5] is commonly utilised in such cases. During the incidence of TM-polarized light on the prism metal interface and reflectance measurement, a sharp dip occurs at either the resonance angle (angular interrogation) or resonance wavelength (spectral interrogation). This phenomenon depends on the adopted interrogation method. The refractive index (RI) of the dielectric (sensing layer) can be accurately determined by understanding the resonance wavelength or angle. Miniature size and measurement portability outside the confines of a laboratory are the important benefits of fibre-optic SPR sensors. These sensors are also used as low-cost components to enhance the multichannel performance of high-throughput screening and remote sensing. Fibre sensors with different geometries are used for selective cladding removal [6], [7], and tapered geometries [8] and as D-shaped fibres [9].The detection accuracy (DA) and sensitivity (S) of thin-layer Ag displays with SPR sensors are superior to those of Au layers because the former feature a larger ($\varepsilon_r/\varepsilon_i$) ratio than the latter, where ε_i and ε_r are the permittivitys imaginary and real sections, respectively, thus accounting for the absorption and reflection of light in the metal [10]. Several preliminary studies on the sensing performance of SPR fibres have shown that PCF and POF should be extensively applied in plasmonic sensors based on pure metallic nanostructures. TFBG and LPG may also be explored to improve the sensing performances of sensor designs[11]. The plasmonic grating configurations of SiO_2 and SiC were introduced for salivary cortisol detection and analyzed on the basis of the on-power-loss spectrum, which leads to the enhancement of sensing performance[12]. Au grating is fabricated on the side surface of a D-shaped optical fibre by using a focused ion beam to improve the S of sensors to the variation in the RI of the environmental liquid [13]. S can be improved as a benefit of the LSPR effect on the Au grating [14]. Fibre sensors with multilayered graphene are used for ethanol detection, and sensing performance is enhanced by enforcing the optimum radiation damping condition in terms of variable Ag layer thickness and temperature in the sensor variants [15]. Various oxides with distinctive crystalline and stoichiometry phases can be formed by Ge. These oxides include hematite ($\alpha - Fe_2O_3$), wustite, maghemite, and magnetite. $\alpha - Fe_2O_3$ is the thermodynamically stable phase of Fe_2O_3. This semiconductor material is inexpensive, nontoxic, abundant in supply, and exhibits excellent thermodynamic stability when subjected to high temperatures [16].Based on an optical perspective, $\alpha - Fe_2O_3$ features a band gap of 2.2 eV in the visible range and a high RI. Hence, $\alpha - Fe_2O_3$ can benefit various optical applications, such as electrochromism, interference filters, photocatalysts, and solar energy conversion [16], [17], [18], [19].$\alpha - Fe_2O_3$ thin films can be developed

Riadh A.Kadhim is with the Institute of Fundamental and Frontier Science (IFFS), University of Electronic Science and Technology of China (UESTC),Chengdu 610054, China; University of Technology, Iraq (e-mail: alazizdl@gmail.com. Liming Yuan, Hao Xu, Jiang Wu ,Zhiming Wang are with the Institute of Fundamental and Frontier Science (IFFS), University of Electronic Science and Technology of China (UESTC),Chengdu 610054, China (Iming_y@uestc.edu.cn ; Hao.xu.15@uestc.edu.cn;jiangwu@uestc.edu.cn;zhmwang@uestc.edu.cn).

by utilising various techniques, such as sputtering [17], [18], [19], [20]. $\alpha - Fe_2O_3$ is an iron-oxide polymorph with low toxicity, high corrosion resistance, air stability, and low cost. These properties are attributed to the compounds coreshell nanostructure with a biphasic formation. $\alpha - Fe_2O_3$ also displays synergistic effects within biosensors or chemicals [21].The potential use of coreshell nanostructures in sensing applications is attributed to their unique catalytic properties and extremely large surface area [22].The development of SPR-based optical fibre arsenic (As[III]) sensor relies on the use of an $\alpha - Fe_2O_3$/SnO_2 coreshell nanostructure (denoted as [α-Fe/Sn] CS) generated via hydrolysis. [23]. Lossy mode resonance (LMR) is a sensing method that is similar to SPR. In LMR, a transparent metal oxide is used instead of a metal layer. An optical fibre LMR-based As(III) sensor is utilised by using coreshell nanostructures ($\alpha - Fe_2O_3$ NPs as the core with SnO_2 as the shell) as the layer for sensing [24].This work proposed improving the S and DA of optical fibre sensors by presenting a D-shaped optical fibre SPR-based sensor with Ag grating-coated $\alpha - Fe_2O_3$. The Ag grating layer showed a sharpened SPR curve dip that allowed the Au layer to retain its DA and S. The oxidation problem of the Ag grating layer in air was addressed through coating with an $\alpha - Fe_2O_3$ layer.$\alpha - Fe_2O_3$ films can be deposited by utilising various techniques, such as magnetron sputtering. $\alpha - Fe_2O_3$ is an iron-oxide polymorph with low toxicity, high corrosion resistance, air stability, and low cost. Additionally, the parameters of bimetallic layer thickness (Ag, $\alpha - Fe_2O_3$) and the gap width between Ag gratings (w_a) and residual cladding thickness (d_r) were optimised to obtain the maximum SPR sensor with the maximum S. This paper is organized as follows. In Section 2, the design and theoretical background of the study are discussed.The performance parameters are elaborated on in Section 3. The results and discussion are provided in Section 5, and conclusions are given in Section 5.

II. DESIGN AND THEORETICAL BACKGOURND

SPWs are created by using fibre SPR sensors via evanescent wave on the fibre surface. Free electrons are then generated on the metal surface. A section of energy from light (incident) is absorbed when the evanescent wave resonates with the SPW, resulting in a reduction in the reflected light energy. Thus, the spectrum will achieve the ultimate peak of absorption resonance. The RI on the medium changes with the resonance peak position. Therefore, the sensors RI can be examined by observing alterations in the resonance peak position.The proposed SPR fibre-optic sensor (figure 1a)was designed through side polishing method with a depth of 0.1 μm to create a plane-sensing area. Ag and $\alpha - Fe_2O_3$ layers were deposited onto the plane surface of the D-shaped fibre optic via pulsed laser deposition or magnetron sputtering. Then, the nanolithography technique was used to fabricate Ag/$\alpha - Fe_2O_3$ gratings. Figure 1b shows the cross-section of the SPR sensor. The core and cladding diameters of the single-mode fibre were 9 and 125μm respectively .The length of the sensing region was L = 1 mm. The width of Ag gratings and the air gaps between gratings are represented by w_g and w_a, respectively. The thicknesses of the $\alpha - Fe_2O_3$ and Ag gratings are represented by d_2 and d_1, respectively. The quantity of residual cladding is represented by d_r. Λ is the grating period, and η = w_g /Λ is the duty cycle.

A. SPR phenomenon

The SPR optical structure featured a metaldielectric interface, which accommodated a p-polarized EM wave that was a SPW running across the interface. Strong light absorption occurred because of the energy transfer during the incidence of a reduction in the reflected light energy.Thus, the spectrum will achieve the attributed to the resulting evanescent wave that was similar to the SPW. The following expressions provide the aforementioned resonance condition[25]:

$$K_{SPW} = K_0(\frac{\varepsilon_{mr} n_s^2}{\varepsilon_{mr} + n_s^2})^{1/2} \quad (1)$$

where K_0 = $\frac{2\pi}{\lambda}$

The propagation constant (KSP) with ε_{mr} as the metal dielectric constant (ε_m)s genuine section is represented by the term on the right. n_s denotes the sensing (dielectric) layers RI. This technique works effectively for sensing distinct variables because the matching condition of this propagation constant exhibits high sensitivity towards light fluctuations within the dielectric constant [25].

B. Fibre Core and Cladding

A step-index single-mode fibre with pure silica as cladding and a silica core (3.1 doped GeO_2) was considered for theoretical modelling. The Sellmeier dispersion relation provides the fibre core and claddings wavelength-dependent RI (n) [26]:

$$n(\lambda) = (1 + \frac{a_1\lambda^2}{\lambda^2 - b_1^2} + \frac{a_2\lambda^2}{\lambda^2 - b_2^2} + \frac{a_3\lambda^2}{\lambda^2 - b_3^2})^{1/2} \quad (2)$$

where the Sellmeier coefficients are represented by b_3, b_2, b_1, a_3, a_2 and a_1, and the wavelength is represented by λ. This study utilised the parameters shown in Table I [26].

C. Dispersion Relationships

Given their remarkable absorption features, silver and gold are commonly utilised in the sensing fields within the structure of SPR sensors. Silver displays a sharper resonance peak than gold and offers excellent DA. Nevertheless, silver shows a high risk to be oxidised within air space. The surface of silver is commonly coated with a sensitive metal oxide to prevent its oxidation and enhance the sensors sensitivity [27]. The Drude dispersion model [28] is used for wavelength dependencies of metal layer dielectric constant.

$$\varepsilon_m(\lambda) = 1 - \frac{\lambda^2\lambda_c}{\lambda_p^2(\lambda_c + i\lambda)} \quad (3)$$

$$\sqrt{\varepsilon_m(\lambda)} = n_m(\lambda) + jk_m(\lambda) \quad (4)$$

where ε_m is the metals complex permittivity, k_m and n_m refer to the imaginary and real sections of the index of metals refraction, respectively, λ_c is the collision wavelength

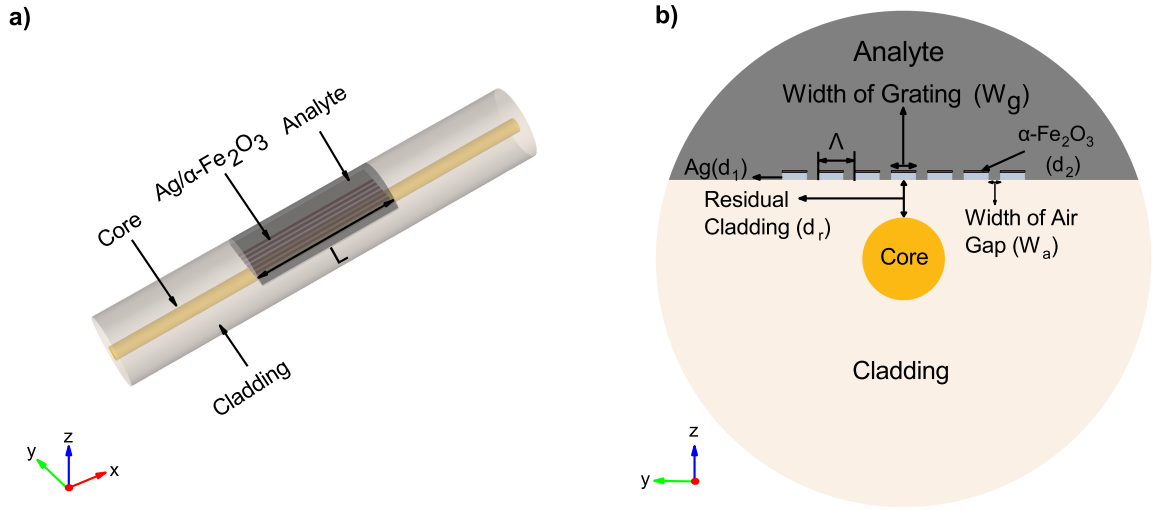

Fig. 1: Schematic of SPR fibre sensor based on silver grating-coated hematite($\alpha - Fe_2O_3$). (a) 3D structure probe. (b) Cross-section of SPR sensor.

TABLE I: Sellmeier coefficients for the fibre core and cladding

coefficients	a_1	a_2	a_3	b_1 (μm)	b_2 (μm)	b_3 (μm)
Cladding (pure silica)	0.6961663	0.4079426	0.8974794	0.0684043	0.1162414	9.896161
Core (3.1 doped GeO_2)	0.7028554	0.4146307	0.8974540	0.0727723	0.1143085	9.896161

associated with losses, and λ_p is the wavelength associated with bulk plasma frequency. Table II lists the values of Au and Ag λ_c and λ_p.

TABLE II: Dispersion coefficients for Au and Ag

dispersion coefficients (μm)	Au	Ag
λ_p	0.16826	0.14541
λ_c	8.9342	17.614

To determine the complex RI of the hematite $\alpha - Fe_2O_3$ layer, reflectance was ascertained by utilising the expression $R = 1 - [Texp(A)]^{1/2}$, whereby A represents layer absorption. The approximation $n = [(1 + R)/(1 - R)] + [((4R)/(1 + R)^2 - (k)2]^{1/2}$ was utilised to ascertain the layer RI (n), in which k refers to the extinction coefficient associated with the absorption coefficient (α) as k = $\alpha\lambda/4$ [29].
Based on transmission function, the amount of power conveyed via power monitors T was calculated and normalised towards the source of power based on the p-polarised light.

$$T = \exp(-\frac{4\pi}{\lambda_0} imag(n_{eff})L) \tag{5}$$

In this case, n_{eff} represents the surface plasmon modes effective index,λ_0 refers to light source wavelength, and L corresponds to the sensing regions length. The plot of the sensor output (SPR response curve) denotes the normalised transmitted power against wavelength. Phase matching between the surface plasmon mode and the optical fibres fundamental mode generates resonance. The SPR response experiences a dip when this resonance condition is reached [30].

III. PERFORMANCE PARAMETERS

The performance of an SPR sensor is affected from two concepts. Firstly, the greatest shift in resonance wavelength ($\Delta\lambda_{res}$) for a particular change (Δn) in the sensing layer RI is recommended. Secondly, the smallest full width at half minimum (FWHM) should be associated with the SPR curves ($\Delta\lambda_{1/2}$). A considerable change could produce a remarkable sensitivity because the resonance wavelength adapts to alterations in the RI of the sensing medium. If Δn alters the RI of the sensing layer, and $\Delta\lambda_{res}$ is the corresponding alteration in resonance wavelength, then the SPR sensors sensitivity is defined as follows [31].

$$S = \frac{\Delta\lambda_{res}}{\Delta n} \tag{6}$$

$$DA = \frac{1}{FWHM} \tag{7}$$

The figure of merit (FOM) of the proposed sensor depends on the sensitivity and full width at half maximum (FWHM) and is defined as follows [32].

$$FOM = \frac{S}{FWHM} \tag{8}$$

The SPR curves depth is proportional to sensitivity, whereas its width is inversely proportional to detection accuracy. A narrow FWHM produces considerable results for detection accuracy. Thus, the performance of any sensor is highly dependent on sensitivity and detection accuracy, aiding in the measurement of resonance wavelength. The factors that affect the S and DA of SPR sensors include surface roughness, quantity of residual cladding and metal layer thickness [27].The transmission dip should be defined in detail to observe the resonance wavelength accurately. Thus, another condition may be integrated over the dip as observation of the FWHM. Occasionally, the FWHM may not be defined given the extremely shallow dip arms. In such cases, FWHM is addressed by adjusting the probe design parameters [33].

IV. RESULTS AND DISCUSSION

The resonant wavelength was affected by the number of Ag gratings. Figure 2a shows the number of Ag gratings as the transmission spectra fluctuated between 5 to 50. No shift occurred in the resonant wavelength when the number of Ag gratings exceeded 20 and 30. As the grating arrays length overrode the fibre core diameter, the number of Ag gratings showed a minimal influence on the response of the sensor to the outer environment [34].When the external RI was high (1.39) and the number of Ag gratings was 5, a secondary peak appeared at a shortened wavelength in addition to the sharp primary resonance peak. This secondary peak was due to a quadrupole resonance that had a different electron oscillation pattern from the primary dipole resonance, resulting in a reduction in the DA of the primary resonance peak. Thus, the number of Ag gratings was set to 20. As shown in figure 2b, reduction in the quantity of residual cladding resulted in a deep and wide SPR curve. Consequently, the detection accuracy decreased, and sensor sensitivity increased. Conversely, the association between the SPR and fundamental mode was weakened when the amount of residual cladding increased, resulting in a shallow SPR dip and narrow width. Finally, the sensitivity decreased, whereas the detection accuracy showed improvement [30].

Figure 3 illustrates the relationship between the external RI and resonant wavelength at various air gap widths and the fixed grating width of w_g = 0.5 μm. The increase in the sensing mediums RI resulted in a nonlinear increase in each air gaps resonance wavelength. The S of the SPR fibre sensor was determined on the basis of the curve slope.The maximum S values of the SPR fibre sensor at the sensing medium RI of 1.39 with the air gap widths of 10, 30, 50, and 70 nm were 4.6, 4.4, 4.2, and 4.0 μm/RIU, respectively. A minor reduction in S was observed with increased gap widths. High S was obtained when the air gap width (w_a) between the gratings was 10 nm. This finding implied the lack of an indefinite increase in the sensors S with the width of air gaps between Ag gratings.

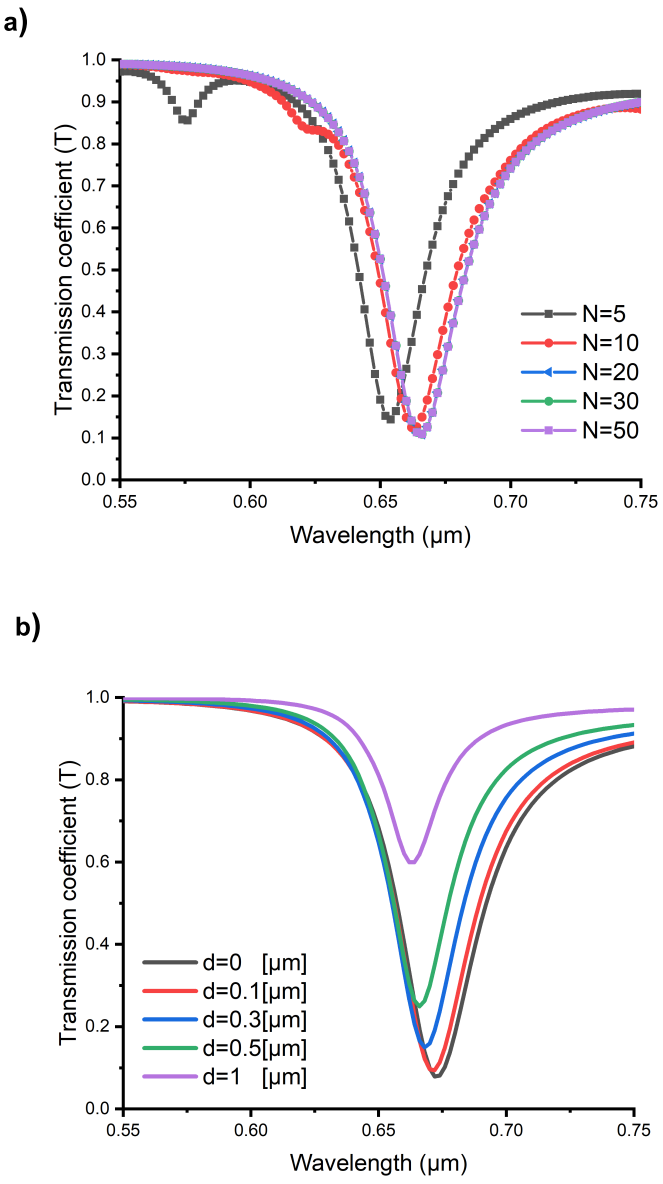

Fig. 2: (a) Spectra of the proposed SPR fibre sensor at various numbers of silver gratings (N); external RI=1.39. (b) Spectra of the proposed SPR at various quantities of residual cladding (d_r).

Figure 4a illustrates the relationship between the wavelength at RI = 1.39 and transmission spectra in terms of the distinct thickness of Ag gratings. The reduced thickness of Ag gratings produced a remarkable dip in SPR, thereby increasing S. With increased Au layer thickness, S increased whereas DA decreased. Thickness increased as DA reached its minimum possible measurable value, resulting in the maximum Au layer thickness of 65 nm. Increased Au layer thickness produced shallow transmission spectra. Occasionally, the DA was lower than its defined limit, as shown in Figure 4b. Therefore, the Ag layer performed better than the Au layer in retaining its DA and S.

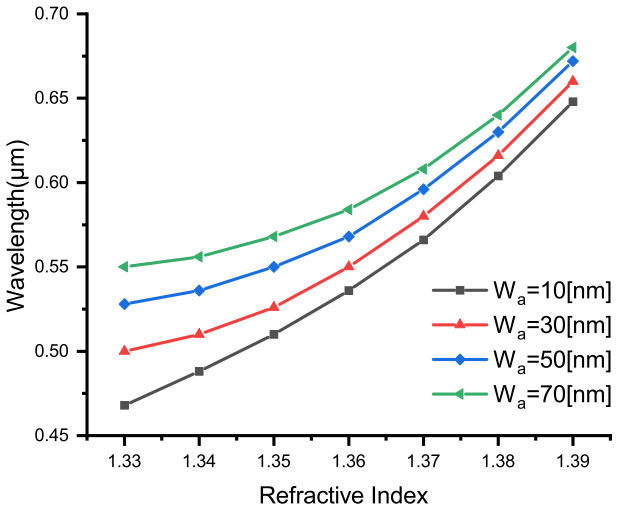

Fig. 3: Relationship between the external RI and resonant wavelength at various air gap widths (w_a).

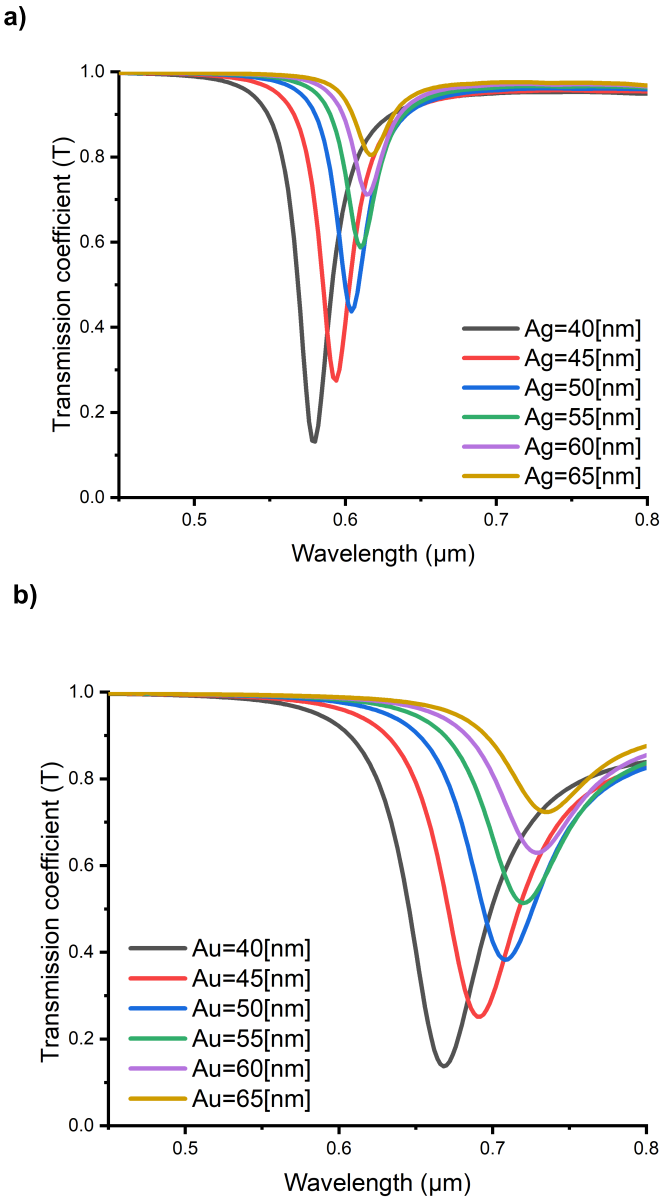

Fig. 4: (a) Relationship between the transmission spectra and wavelength at RI = 1.39 and specific thicknesses of the Ag . (b) Relationship between the transmission spectra and wavelength at RI = 1.39 and specific thicknesses of the Au layers.

As shown in figure5, the SPR transmission spectra changed in accordance with the external RI when the gap width between gratings spanned 10 nm, and 20 silver gratings were used. When the silver grating thickness was 45 nm, and RI was changed from 1.33 to 1.39, the maximum SPR sensitivity sensor reached 4.6 μm/RIU, whereas the DA measured 29.12 μm^{-1}. Thus, the number of silver gratings and gap width (w_a) between the gratings were optimised

The effect of $\alpha - Fe_2O_3$ on the sensor S was studied by lining the outside of Ag gratings with $\alpha - Fe_2O_3$. The sensor model was set up by using a Ag grating with a 0.5 μm width and 10 nm air gap width. Figure6a shows the transmission spectrum of the SPR fibre sensor with a wavelength of 952 nm and RI of 1.39. The intensity of the electric field was illustrated via the finite element method for the sensor structure of Ag/$\alpha - Fe_2O_3$ grating film with 12 nm layer of $\alpha - Fe_2O_3$ coated on the 45 nm-thick Ag layer. During SPR, the wave vectors of the surface plasmon and incident EM waves matched with each other.Energy from the core transferred to the interface of the $\alpha - Fe_2O_3$ medium, thereby enhancing the strength of the electric field on the $\alpha - Fe_2O_3$ medium interface. Consequently, the grating surfaces electric field strength significantly increased. As shown in Figure 6b, the evanescent field distribution and mixed medium RI were altered by $\alpha - Fe_2O_3$.

Figure 7a shows the transmission spectra of the SPR fibre sensors at a specific $\alpha - Fe_2O_3$ thickness with RI of 1.39, Ag grating width of 0.5 μm, and air gap width of 10 nm. With increased thickness, the SPR sensors wavelength moved toward a long wavelength, and the spectrum further deepened. The thickness of the $\alpha - Fe_2O_3$ layer was changed from 0 nm to 14 nm to determine its optimum thickness and enhance the S of the proposed SPR fibre sensor. The absorption coefficient (α) of the $\alpha - Fe_2O_3$ layer increased with decreased thickness. This behavior affected the decreasing variation in shift resonance wavelength ($\Delta\lambda_{res}$), thereby decreasing S. Accordingly, S decreased to 5.0 μm/RIU when $\alpha - Fe_2O_3$ thickness was 14 nm. As shown in Figure 7b, the $\alpha - Fe_2O_3$ thickness of 12 nm produced the highest S. Thus, the $\alpha - Fe_2O_3$ thickness of the proposed SPR sensor was set to 12 nm.

The SPR curves depth is proportional to S, whereas its width is inversely proportional to DA. A narrow FWHM produced desirable results for DA. The performance of any sensor is highly dependent on sensitivity and DA. In Figure 8, the SPR fibre sensors spectra with RI as the number of gratings were fixed at 20. The gap width between gratings was 10 nm, the Ag layer thickness was 45 nm, and $\alpha - Fe_2O_3$ thickness was

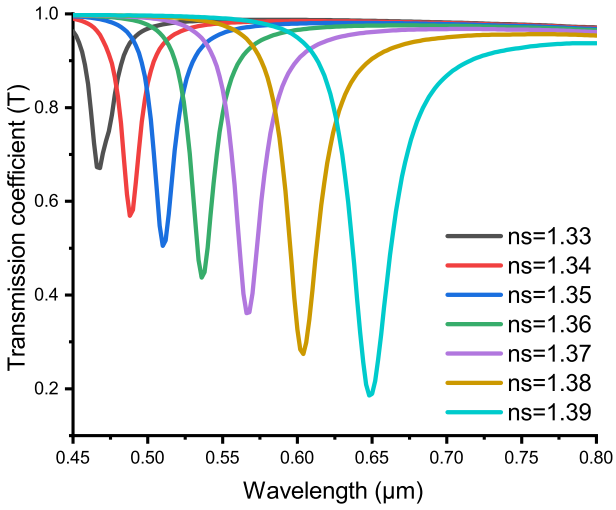

Fig. 5: Spectra of the proposed SPR fibre sensor with varied external RIs, 20 silver gratings, 10 nm gap width between gratings and silver thickness of 45 nm.

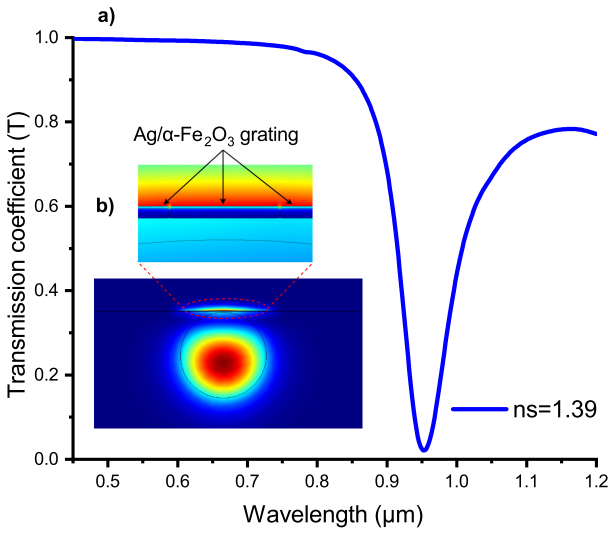

Fig. 6: (a) Spectrum of the proposed SPR fibre sensor at external RI of 1.39. (b) Electric field of Ag/$\alpha - Fe_2O_3$ grating SPR sensor.

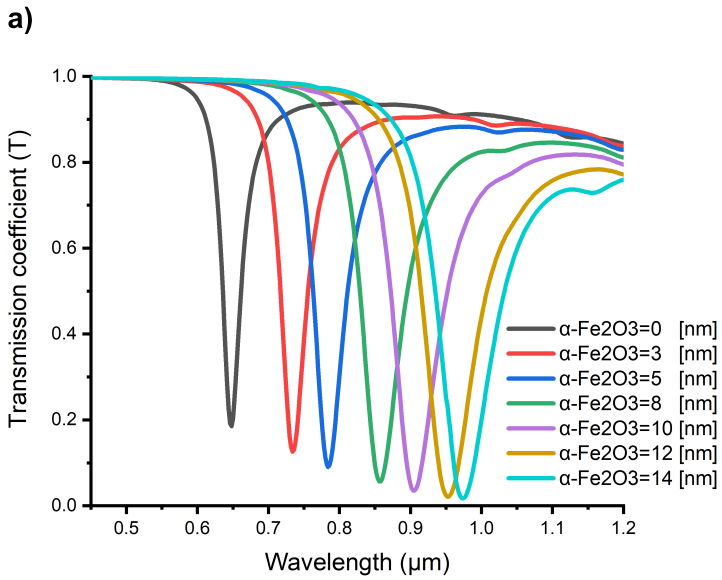

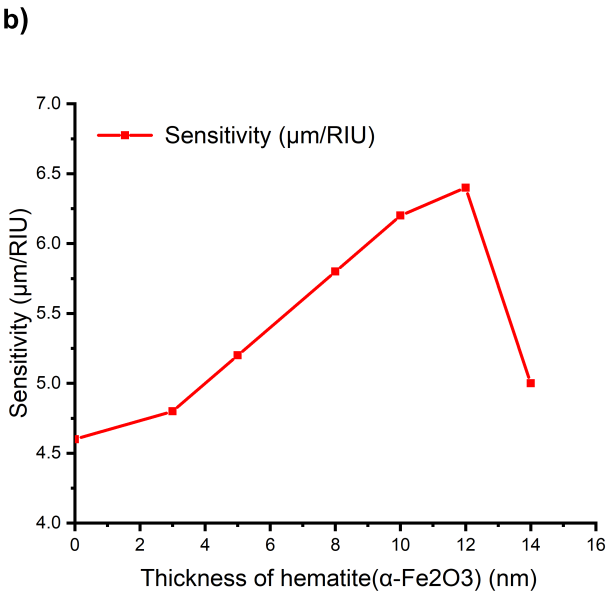

Fig. 7: (a) Spectra of the proposed SPR fibre sensor with varied hematite thicknesses at an external RI of 1.39. (b) Variation in sensitivity with different thicknesses of hematite.

12 nm. At Ag/$\alpha - Fe_2O_3$ grating thickness of Ag 45 nm + $\alpha - Fe_2O_3$ 12 nm and increased external RI from 1.33 to 1.39, the SPR curve dip deepened and widened. Thus, the sensitivity was enhanced, but DA was decreased, especially at high external RI.

Figure 9(a,b) illustrates that the relationship between the external RI and resonant wavelength varied with different thicknesses of $\alpha - Fe_2O_3$. Au and Ag layer thicknesses were set at 45 nm, the external RI and $\alpha - Fe_2O_3$ thickness increased, and the resonance wavelength was diverted toward the long-wave direction.The S of the SPR fibre sensor with various thicknesses of the sensing layer regions could be determined on the basis of the curve slope. The minimum S values of the SPR fibre sensor with the sensing medium RI of 1.33 and 0, 3, 5, 8, 10, and 12 nm $\alpha - Fe_2O_3$ thicknesses were 2.2, 2.6, 1.8, 2.1, 2.0, and 2.4 μm/RIU, respectively. The maximum S values of the SPR fibre sensors with the sensing medium RI of 1.39 were 4.6, 4.8, 5.6, 5.8, 6.2, and 6.4 μm/RIU .The S of the SPR fibre sensor was affected by metal layer thickness (Ag), the gap width between the Ag gratings (w_a), and residual cladding thickness (d_r). All of these parameters were optimised to obtain the maximum SPR S of the sensor, which reached 4.6 μm/RIU. When a $\alpha - Fe_2O_3$ layer was coated on the Ag grating, the maximum SPR S of the sensor

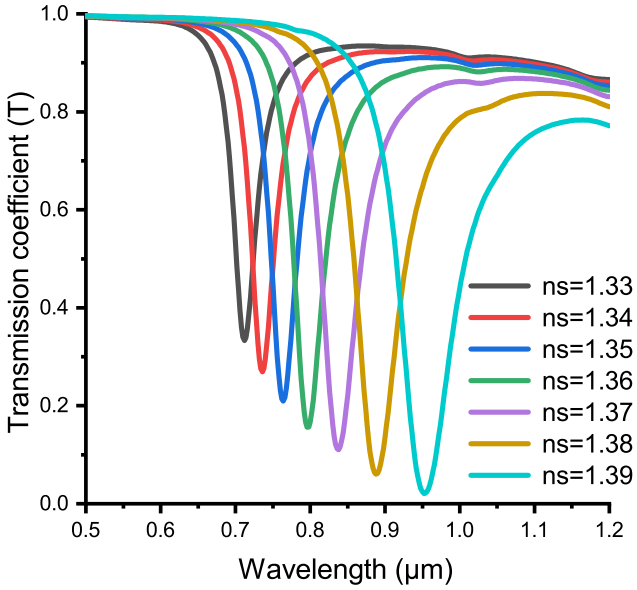

Fig. 8: : Spectra of the proposed SPR fibre sensor with varied external RIs and (45+12) nm thick Ag/$\alpha - Fe_2O_3$ grating

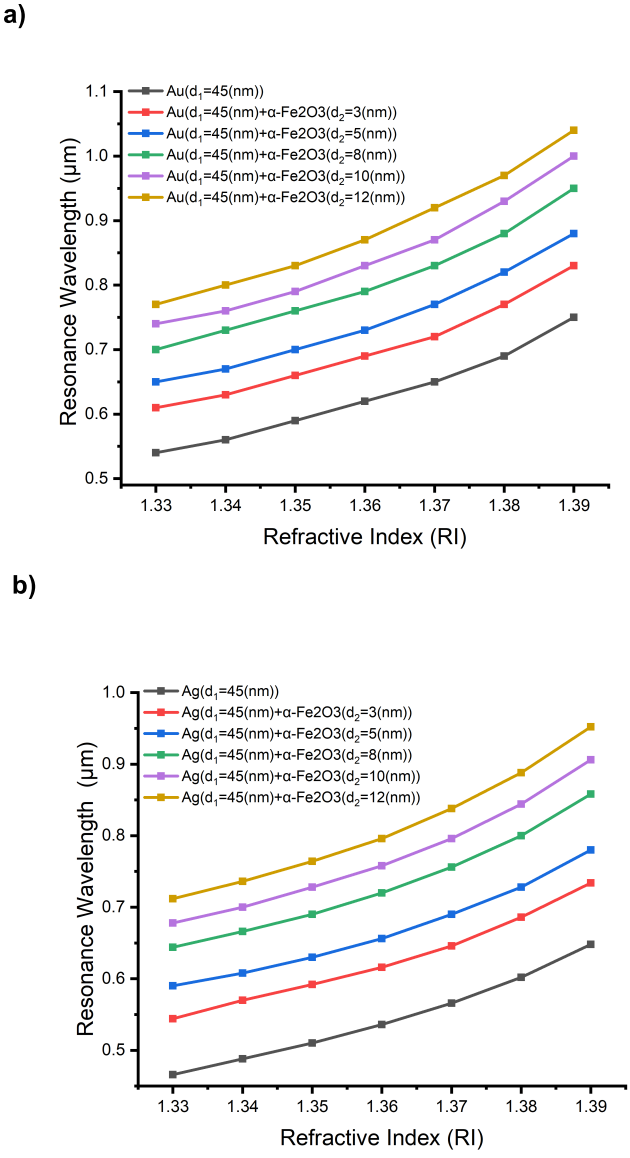

Fig. 9: Relationship between the varied external RIs and resonant wavelength (a) Au. (b) Ag .

reached 6.4 μm/RIU. The introduction of $\alpha - Fe_2O_3$ as a sensing layer highly promoted the effectiveness and S of the SPR sensor .

Table III shows that when a $\alpha - Fe_2O_3$ layer was coated on the Ag grating with a thickness of 0-14 nm and the Ag layer thickness was fixed at 45 nm, S increased to 6.4 μm/RIU at the thickness of 12 nm and the external RI reached 1.39. S decreased to 5.0 μm/RIU when the $\alpha - Fe_2O_3$ thickness was 14 nm. DA and FOM decreased to 7.56 μm^1 and 37.8 RIU^{-1}, respectively, because of the increased $\alpha - Fe_2O_3$ thickness layer of the SPR fibre sensor and the wide FWHM, which was the inverse of DA and FOM. However, S improved at high RI, where S was the key concern. The performance of the proposed D-shaped optical fibre equipped with $\alpha - Fe_2O_3$-coated Ag gratings was compared with that of other sensors reported in the literature. The results are shown in Table IV.

V. CONCLUSION

Sensor sensitivity under the premise of calculable FWHM increased with increased $\alpha - Fe_2O_3$ thickness. Only the effects of the various thicknesses of $\alpha - Fe_2O_3$ on the S of SPR sensors and DA were studied. A single-mode D-shaped optical fibre sensor equipped with $\alpha - Fe_2O_3$-coated Ag gratings was proposed and simulated to observe the effects of $\alpha - Fe_2O_3$thickness on sensor S. The model was optimised and constructed by using COMSOL Multiphysics software. The thickness and number of Ag gratings were 45 nm and 20, respectively; the gap width between gratings was 10 nm; and $\alpha - Fe_2O_3$ thickness was 12 nm. The simulation outcomes demonstrated that the S of the sensor increased when the $\alpha - Fe_2O_3$ thickness was 0-12 nm. The RI was within the range of 1.33-1.39 when the gap width of Ag gratings was 10 nm. The proposed sensors minimum response S reached 2.4 μm/RIU, and its maximum response S was 6.4 μm/RIU when the $\alpha - Fe_2O_3$ layer thickness was 12 nm. Finally, the SPR sensors S can be significantly enhanced by the bimetallic grating layer (Ag/$\alpha - Fe_2O_3$). A theoretical basis was provided for the development of SPR sensors with high S. Therefore, the SPR fibre sensor is a good candidate for bio/chemical applications given its high S and the advantage conferred by the bimetallic grating layer (Ag/ $\alpha - Fe_2O_3$).By presenting simulation results, we have proved that the influence of our approach through a D-shaped optical fibre SPR-based sensor with the bimetallic grating layer. In future work directions the actual execution for experimental design is very important for testing the proposed optical fiber structure .

TABLE III: sensitivity , DA and FOM at different hematite thicknesses

$(\alpha - Fe_2O_3)$Thickness (nm)	$\Delta\lambda_{SPR}$ (μm)	Δn(RIU)	Sensitivity (μm/RIU) (RI=1.39)	DA (μm^{-1}) (RI=1.39)	FOM (RIU^{-1}) (RI=1.39)
0	0.046	0.01	4.6	29.12	133.9
3	0.048	0.01	4.8	20.72	99.4
5	0.056	0.01	5.6	17.25	96.6
8	0.058	0.01	5.8	12.99	75.3
10	0.062	0.01	6.2	10.82	67.0
12	0.064	0.01	6.4	8.83	56.5
14	0.050	0.01	5.0	7.56	37.8

TABLE IV: Comparison with D-shape SPR sensors.

Sensor Type	Material	RI Range (RIU)	Sensitivity (nm/RIU)	Ref.
D-shaped fibre	Ag+GO	1.30 to 1.34	833.33	[35]
D-shaped fibre	Au	1.35 to 1.43	925	[36]
D-shaped PCF	Au	1.36 to 1.38	3340	[37]
D-shaped fibre	G+ITO	1.33 to 1.35	5700	[38]
This work	Ag+$\alpha - Fe_2O_3$	1.33 to 1.39	6400	

REFERENCES

[1] Khalil Tamersit and Fayçal Djeffal. Double-gate graphene nanoribbon field-effect transistor for dna and gas sensing applications: simulation study and sensitivity analysis. *IEEE Sensors Journal*, 16(11):4180–4191, 2016.

[2] Jiří Homola and Marek Piliarik. Surface plasmon resonance (spr) sensors. In *Surface plasmon resonance based sensors*, pages 45–67. Springer, 2006.

[3] Qingling Ouyang, Shuwen Zeng, Li Jiang, Liying Hong, Gaixia Xu, Xuan-Quyen Dinh, Jun Qian, Sailing He, Junle Qu, Philippe Coquet, et al. Sensitivity enhancement of transition metal dichalcogenides/silicon nanostructure-based surface plasmon resonance biosensor. *Scientific reports*, 6:28190, 2016.

[4] Briliant Adhi Prabowo, Agnes Purwidyantri, and Kou-Chen Liu. Surface plasmon resonance optical sensor: A review on light source technology. *Biosensors*, 8(3):80, 2018.

[5] Pradeep Kumar Maharana, Rajan Jha, and Srikanta Palei. Sensitivity enhancement by air mediated graphene multilayer based surface plasmon resonance biosensor for near infrared. *Sensors and Actuators B: Chemical*, 190:494–501, 2014.

[6] RC Jorgenson and SS Yee. A fiber-optic chemical sensor based on surface plasmon resonance. *Sensors and Actuators B: Chemical*, 12(3):213–220, 1993.

[7] A Dıez, MV Andres, and JL Cruz. In-line fiber-optic sensors based on the excitation of surface plasma modes in metal-coated tapered fibers. *Sensors and Actuators B: Chemical*, 73(2-3):95–99, 2001.

[8] Kazuyoshi Kurihara, Hiroyuki Ohkawa, Yuzuru Iwasaki, Tatsuya Tobita, Osamu Niwa, and Koji Suzuki. Microscale fiber-optic spr sensors based on nsom technology. In *Micro Total Analysis Systems 2001*, pages 353–354. Springer, 2001.

[9] Nasim Rezaei and Alireza Yahaghi. A high sensitivity surface plasmon resonance d-shaped fiber sensor based on a waveguide-coupled bimetallic structure: modeling and optimization. *IEEE Sensors Journal*, 14(10):3611–3615, 2014.

[10] BD Gupta and Anuj K Sharma. Sensitivity evaluation of a multi-layered surface plasmon resonance-based fiber optic sensor: a theoretical study. *Sensors and Actuators B: Chemical*, 107(1):40–46, 2005.

[11] Anuj Kumar Sharma and Carlos Marques. Design and performance perspectives on fiber optic sensors with plasmonic nanostructures and gratings: A review. *IEEE Sensors Journal*, 19(17):7168–7178, 2019.

[12] Ankit Kumar Pandey, Anuj K Sharma, and Carlos Marques. On the application of sio2/sic grating on ag for high-performance fiber optic plasmonic sensing of cortisol concentration. *Materials*, 13(7):1623, 2020.

[13] Hai-Tao Yan, Qi Liu, Yang Ming, Wei Luo, Ye Chen, and Yan-qing Lu. Metallic grating on a d-shaped fiber for refractive index sensing. *IEEE Photonics Journal*, 5(5):4800706–4800706, 2013.

[14] Tulika Khanikar and Vinod Kumar Singh. Gold grating assisted spr based d-shaped single mode fiber for detection of liquid refractive index. *Optical and Quantum Electronics*, 51(9):296, 2019.

[15] Anuj K Sharma, Baljinder Kaur, and Carlos Marques. Simulation study on fluoride fiber spr sensor with multilayer arrangements of graphene under thermal variation of radiation damping in nir. In *Optical Sensing and Detection VI*, volume 11354, page 113542F. International Society for Optics and Photonics, 2020.

[16] Niclas Beermann, Lionel Vayssieres, Sten-Eric Lindquist, and Anders Hagfeldt. Photoelectrochemical studies of oriented nanorod thin films of hematite. *Journal of the Electrochemical Society*, 147(7):2456–2461, 2000.

[17] Eric L Miller, Daniela Paluselli, Bjorn Marsen, and Richard E Rocheleau. Low-temperature reactively sputtered iron oxide for thin film devices. *Thin Solid Films*, 466(1-2):307–313, 2004.

[18] L Dghoughi, B Elidrissi, C Bernede, M Addou, M Alaoui Lamrani, M Regragui, and H Erguig. Physico-chemical, optical and electrochemical properties of iron oxide thin films prepared by spray pyrolysis. *Applied Surface Science*, 253(4):1823–1829, 2006.

[19] Yong Jun Park, KMA Sobahan, and Chang Kwon Hwangbo. Optical and structural properties of fe2o3 thin films prepared by ion-beam assisted deposition. *Surface and Coatings Technology*, 203(17-18):2646–2650, 2009.

[20] K Mörl, U Röpke, B Knappe, J Lehmann, R Perthel, and H Schröder. Optical properties of sputtered fe2o3 films. *Thin Solid Films*, 60(1):49–53, 1979.

[21] Guohong Qiu, Hui Huang, Homer Genuino, Naftali Opembe, Lisa Stafford, Saminda Dharmarathna, and Steven L Suib. Microwave-assisted hydrothermal synthesis of nanosized α-fe2o3 for catalysts and adsorbents. *The Journal of Physical Chemistry C*, 115(40):19626–19631, 2011.

[22] Andrey V Nomoev, Sergey P Bardakhanov, Makoto Schreiber, Dashima G Bazarova, Nikolai A Romanov, Boris B Baldanov, Bair R Radnaev, and Viacheslav V Syzrantsev. Structure and mechanism of the formation of core-shell nanoparticles obtained through a one-step gas-phase synthesis by electron beam evaporation. *Beilstein journal of nanotechnology*, 6(1):874–880, 2015.

[23] Sonika Sharma and Banshi Dhar Gupta. Fiber optic surface-plasmon-resonance-based highly sensitive arsenic sensor prepared using α-fe 2 o 3/sno 2 core-shell nanostructure with optimized probe parameters. *Applied optics*, 57(36):10466–10473, 2018.

[24] Sonika Sharma and Banshi D Gupta. Lossy mode resonance-based fiber optic sensor for the detection of as (iii) using α– fe 2 o 3 core–shell nanostructures. *IEEE Sensors Journal*, 18(17):7077–7084, 2018.

[25] Anuj K Sharma, Rajan Jha, and BD Gupta. Fiber-optic sensors based on surface plasmon resonance: a comprehensive review. *IEEE Sensors Journal*, 7(8):1118–1129, 2007.

[26] Jeeban Kumar Nayak and Rajan Jha. Numerical simulation on the

performance analysis of a graphene-coated optical fiber plasmonic sensor at anti-crossing. *Applied optics*, 56(12):3510–3517, 2017.

[27] Yusser Al-Qazwini, ASM Noor, PT Arasu, and AR Sadrolhosseini. Investigation of the performance of an spr-based optical fiber sensor using finite-difference time domain. *Current Applied Physics*, 13(7):1354–1358, 2013.

[28] Sarika Singh and BD Gupta. Simulation of a surface plasmon resonance-based fiber-optic sensor for gas sensing in visible range using films of nanocomposites. *Measurement Science and Technology*, 21(11):115202, 2010.

[29] Pawan Kumar, Nitin Rawat, Da-Ren Hang, Heung-No Lee, and Rajesh Kumar. Controlling band gap and refractive index in dopant-free α-fe 2 o 3 films. *Electronic Materials Letters*, 11(1):13–23, 2015.

[30] Yusser Al-Qazwini, PT Arasu, and ASM Noor. Numerical investigation of the performance of an spr-based optical fiber sensor in an aqueous environment using finite-difference time domain. In *2011 2nd International Conference on Photonics*, pages 1–4. IEEE, 2011.

[31] M Salari and HR Askari. Theoretical investigation of absorption and sensitivity of nano-plasmonic fiber optic sensors. *Optics & Laser Technology*, 48:315–325, 2013.

[32] M Saifur Rahman, Shaikh Sumit Noor, MS Anower, Lway Faisal Abdulrazak, Md Maksudur Rahman, and KA Rikta. Design and numerical analysis of a graphene-coated fiber-optic spr biosensor using tungsten disulfide. *Photonics and Nanostructures-Fundamentals and Applications*, 33:29–35, 2019.

[33] Akhilesh Kumar Mishra, Satyendra Kumar Mishra, and Rajneesh Kumar Verma. Graphene and beyond graphene mos2: a new window in surface-plasmon-resonance-based fiber optic sensing. *The Journal of Physical Chemistry C*, 120(5):2893–2900, 2016.

[34] Haiwei Fu, Min Zhang, Jijun Ding, Jie Wu, Yi Zhu, Huidong Li, Qiqi Wang, and Chong Yang. A high sensitivity d-type surface plasmon resonance optical fiber refractive index sensor with graphene coated silver nano-columns. *Optical Fiber Technology*, 48:34–39, 2019.

[35] Iraj S Amiri, Siti Anis Khairani Alwi, Sofiah Atirah Raya, Nur Ainaa Mardhiah Zainuddin, Nurul Syazwani Rohizat, MS Mani Rajan, and Rozalina Zakaria. Graphene oxide effect on improvement of silver surface plasmon resonance d-shaped optical fiber sensor. *Journal of Optical Communications*, 2019.

[36] Yu Ying, Jiakai Wang, Nan Hu, Ke Xu, Liangliang Sun, and Guangyuan Si. Determination of refractive index using surface plasmon resonance (spr) and rigorous coupled wave analysis (rcwa) with a d-shaped optical fiber and a nano-gold grating. *Instrumentation Science & Technology*, 48(4):376–385, 2020.

[37] Junjie Lu, Yan Li, Yanhua Han, Yi Liu, and Jianmin Gao. D-shaped photonic crystal fiber plasmonic refractive index sensor based on gold grating. *Applied optics*, 57(19):5268–5272, 2018.

[38] Amrit Patnaik, K Senthilnathan, and Rajan Jha. Graphene-based conducting metal oxide coated d-shaped optical fiber spr sensor. *IEEE Photonics Technology Letters*, 27(23):2437–2440, 2015.